#### **OPEN ACCESS**



# On the Likely Dynamical Origin of GW191109 and Binary Black Hole Mergers with Negative Effective Spin

Rachel C. Zhang <sup>1,2</sup>, Giacomo Fragione <sup>1,2</sup>, Chase Kimball <sup>1,2</sup>, and Vicky Kalogera <sup>1,2</sup> Department of Physics & Astronomy, Northwestern University, Evanston, IL 60208, USA

<sup>2</sup> Center for Interdisciplinary Exploration & Research in Astrophysics (CIERA), Northwestern University, Evanston, IL 60208, USA; rczhang@u.northwestern.edu

\*Received 2023 February 14; revised 2023 June 23; accepted 2023 June 26; published 2023 August 21

#### **Abstract**

With the growing number of binary black hole (BBH) mergers detected by LIGO/Virgo/KAGRA, several systems have become difficult to explain via isolated binary evolution, having components in the pair-instability mass gap, high orbital eccentricities, and/or spin–orbit misalignment. Here we focus on GW191109\_010717, a BBH merger with component masses of  $65^{+11}_{-11}$  and  $47^{+15}_{-13}$   $M_{\odot}$  and an effective spin of  $-0.29^{+0.42}_{-0.31}$ , which could imply a spin–orbit misalignment of more than  $\pi/2$  rad for at least one of its components. Besides its component masses being in the pair-instability mass gap, we show that isolated binary evolution is unlikely to reproduce the proposed spin–orbit misalignment of GW191109 with high confidence. On the other hand, we demonstrate that BBHs dynamically assembled in dense star clusters would naturally reproduce the spin–orbit misalignment and masses of GW191109 and the rates of GW191109-like events if at least one of the components were to be a second-generation BH. Finally, we generalize our results to all events with a measured negative effective spin, arguing that GW200225 also has a likely dynamical origin.

Unified Astronomy Thesaurus concepts: Gravitational wave sources (677); Black holes (162)

# 1. Introduction

The LIGO/Virgo/KAGRA (LVK) Collaboration has recently released the third Gravitational Wave Transient Catalog (The LIGO Scientific Collaboration et al. 2021), which has brought the number of candidate binary black hole (BBH) mergers to more than 90 events, transforming our understanding of BHs and gravitational-wave (GW) physics (Abbott et al. 2021a, 2021b). With the upcoming fourth observational run and the next-generation observatories, such as LISA (Consortium et al. 2013), the Einstein Telescope (Maggiore et al. 2020), and Cosmic Explorer (Reitze et al. 2019), the number of GW detections will continue to grow quickly.

Despite the growing population of detected BH mergers, their origin is still highly uncertain. Two main formation channels have been discussed to explain the origin of merging compact objects: isolated binary evolution (e.g., Paczynski 1976; van den Heuvel 1976; Tutukov & Yungelson 1993; Belczynski et al. 2002; Kalogera et al. 2007; Dominik et al. 2012, 2013; Postnov & Yungelson 2014; Belczynski et al. 2016b, 2016; Stevenson et al. 2017; van den Heuvel et al. 2017; Giacobbo & Mapelli 2018; Neijssel et al. 2019; Spera et al. 2019; Bavera et al. 2021) and dynamical assembly in dense stellar environments (e.g., Portegies Zwart & McMillan 2000; Rodriguez et al. 2015; Askar et al. 2017; Banerjee 2017, 2018a, 2018b; Fragione & Kocsis 2018; Samsing & D'Orazio 2018; Samsing 2018; Di Carlo et al. 2019; Kremer et al. 2020; Fragione & Banerjee 2021). Subchannels of these two broad categories include chemically homogeneous evolution of close binaries (e.g., de Mink et al. 2009; de Mink & Mandel 2016; Mandel & de Mink 2016;

Original content from this work may be used under the terms of the Creative Commons Attribution 4.0 licence. Any further distribution of this work must maintain attribution to the author(s) and the title of the work, journal citation and DOI.

Marchant et al. 2016), hierarchical triple and quadruple systems (e.g., Antonini & Perets 2012; Hoang et al. 2018; Fragione et al. 2019; Martinez et al. 2020; Hamers et al. 2021; Martinez et al. 2022), and formation in disks of active galactic nuclei (AGN; e.g., Bartos et al. 2017; Tagawa et al. 2018, 2020).

The isolated binary evolution and dynamical channels can be distinguished through several characteristic features. In the former case, merging BBHs may have component masses up to about  $45 M_{\odot}$ , as dictated by pair-instability physics (e.g., Heger & Woosley 2002; Woosley et al. 2007; Farmer et al. 2019). Moreover, merging BHs have spins preferentially aligned with the orbital angular momentum (implying a positive effective spin), no residual eccentricity at 10 Hz, and mass ratios close to unity (Kalogera 2000; Dominik et al. 2013; Samsing 2018). On the other hand, BBH mergers catalyzed by dynamical encounters in dense star clusters have an isotropic orientation of spins relative to the orbital angular momentum (implying a symmetric distribution of the effective spin around zero) and a broader spectrum of eccentricities in the LVK frequency band but still have mass ratios preferentially close to unity (Rodriguez et al. 2016, 2018; Samsing 2018; Rodriguez et al. 2019; Martinez et al. 2022). Importantly, the component masses of merging BHs can exceed the limit imposed by pairinstability physics if they are the remnant of a hierarchical merger (e.g., Antonini et al. 2019; Fragione & Silk 2020; Mapelli et al. 2021; Fragione et al. 2022).

In this paper, we focus on GW191109, the detected BBH merger with 90.6% of its effective inspiral spin distribution in the negative regime, as shown in Figure 1.<sup>3</sup> Effective inspiral spin is defined as  $\chi_{\rm eff} \equiv (m_1\chi_1 + m_2\chi_2)/(m_1 + m_2)$ , with  $m_i$  and  $\chi_i$  (i=1,2) being the components' masses and spins. This BBH merger event has primary and secondary masses of  $65^{+11}_{-11}$  and  $47^{+15}_{-13}$   $M_{\odot}$ , respectively, and an effective spin of

<sup>&</sup>lt;sup>3</sup> Data origin: the LIGO Scientific Collaboration et al. (2023). Software: Hoy & Raymond (2021).

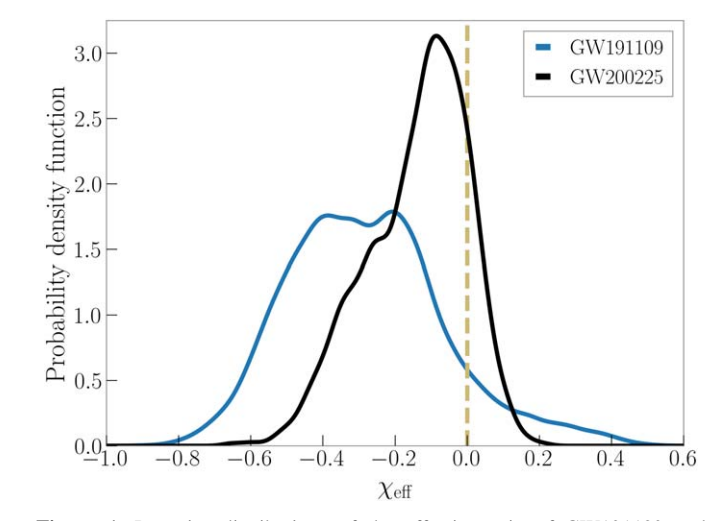


**Figure 1.** Posterior distributions of the effective spin of GW191109 and GW200225\_060421 derived from the PEsummary package by Hoy & Raymond (Hoy 2021) using the open data from the LIGO Scientific Collaboration et al. (2023). The probability of a negative effective spin is about 90.6% and 86.7% for GW191109 and GW200225\_060421, respectively.

 $-0.29_{-0.31}^{+0.42}$ , which implies a spin-orbit misalignment of more than 90° for at least one of its components. The posterior distribution of the effective spin of GW191109 is shown in Figure 1, along with that of GW200225\_060421, the BBH merger event with 86.7% of its effective inspiral spin distribution lying in the negative regime (The LIGO Scientific Collaboration et al. 2021). We argue that the spin orientation is a strong indicator of isolated binary or dynamical formation for GW191109 and, in general, any BBH merger with a negative value of its effective spin. We note that the observed effective spin distribution can be affected by glitches, and a glitch was found in the Livingston data for GW191109 (Davis et al. 2022). Thus, we acknowledge the uncertainties for this measurement and further discuss this in Section 4. We also note that the effective inspiral spin distribution of GW191109 may still be consistent with  $\chi_{\rm eff} \approx 0$  and could be affected by statistical fluctuations and/or model misspecification, which might not entirely rule out the possibility that all events could be explained by isolated binary formation (Galaudage et al. 2021; Roulet et al. 2021; Tong et al. 2022). However, we note that beyond the effective spin, the measured high masses and inferred merger rate also point toward a likely dynamical origin for GW191109, as explained in Section 3.

Our paper is organized as follows. In Section 2, we summarize the GW events with characteristic features that indicate an unlikely isolated binary origin. In Section 3, we tailor our discussion to GW191109 and show that isolated binary evolution is very unlikely to produce GW191109-like events, while dynamics can easily explain its component masses, effective spin, and merger rates. We conclude and generalize our results in Section 4.

### 2. BBHs with an Unlikely Origin in Field Binaries

Here we review BBH mergers that have been discussed to have an unlikely origin as isolated binaries.

1. Masses in the pair-instability mass gap range. The BHs with masses in the range of  $\sim 50-120\,M_\odot$  (depending on the progenitor metallicity) are not expected to be formed from stellar collapse due to runaway pair-instability processes

- (e.g., Fowler & Hoyle 1964; Bond et al. 1984; Heger & Woosley 2002; Woosley et al. 2007; Woosley 2017; Farmer et al. 2019). The merger event GW190521 has component masses of about 90 and  $60 M_{\odot}$ , nominally in the pairinstability mass gap. These masses can be naturally produced in dense stellar environments if these BHs are the remnants of a previous merger event (e.g., Miller & Hamilton 2002; Antonini & Rasio 2016; Gerosa & Berti 2017; Rodriguez et al. 2019; Fragione et al. 2020; Kimball et al. 2021) or in AGN disks through subsequent mergers and gas accretion (e.g., Tagawa et al. 2020, 2020, 2020). Other candidate BBH events with at least one component BH in this upper mass gap range include GW190519\_153544, GW190602\_ 175927, GW190706\_222641, and GW200220\_061928 (Abbott et al. 2021c; The LIGO Scientific Collaboration et al. 2021).
- 2. Unequal mass ratios. Both isolated binaries and cluster dynamics produce BBH mergers that preferentially have mass ratios close to unity (e.g., Dominik et al. 2013; Belczynski et al. 2016; Rodriguez et al. 2016, 2019). However, hierarchical mergers in dense star clusters can naturally produce smaller mass ratios (e.g., Fragione et al. 2022). Detected BBH merger GW190412 has a nearly 4:1 mass ratio, which could easily be explained as a third-generation merger in a massive star cluster (Rodriguez et al. 2020). Other possibilities include a merger in a hierarchical triple, where the inner binary is driven to a merger by the Lidov–Kozai cycles imposed by the tidal field of the tertiary (Su et al. 2021; Martinez et al. 2022), or subsequent mergers in AGN disks (e.g., Tagawa et al. 2020, 2020, 2020).
- 3. Nonzero orbital eccentricities. BBHs tend to have zero eccentricity through isolated binary evolution. This is because orbits tend to circularize to minimize energy (Peters 1964), and merger timescales in isolated binary evolution are long enough for circularization to happen. However, in a dense stellar cluster, highly eccentric BBHs are formed during few-body interactions of BH systems. Specifically,  $\sim$ 5% of all BBH mergers from globular clusters are likely to have an eccentricity  $\geq 0.1$  in the LVK frequency band (Samsing 2018). Another possibility to create merger events with large eccentricities is through Lidov-Kozai cycles in hierarchical systems (e.g., Fragione et al. 2019). Gayathri et al. (2022) used numerical relativity simulations to justify GW190521 as a potential highly eccentric BBH, and Romero-Shaw et al. (2022) argued that both GW191109 and GW200208 have a nonnegligible eccentricity in the LVK detection band.
- 4. Negative effective inspiral spin parameter. Isolated binary evolution leads to a preferential alignment between the BH spins and the binary orbital angular momentum, typically implying a positive value of the effective spin (Kalogera 2000). A positive value of the effective spin may also be preferred by the AGN disk channel if the radial migration of BHs is inefficient (e.g., Tagawa et al. 2020). Dynamical assembly in dense star clusters (Rodriguez et al. 2016) and mergers in hierarchical systems (Martinez et al. 2022) lead to an isotropic distribution of the effective spin around zero. Therefore, a system with a negative value of the effective spin is unlikely to originate in field binaries and AGN

disks (for details, see Section 3). Currently, the GW BBH events that show a likely negative observed  $\chi_{\rm eff}$  are GW191109 (see Section 3) and GW200225 (see Section 4).

### 3. The Case of GW191109

In this section, we show that the likely origin of GW191109 is dynamical assembly in dense star clusters. We use the properties of mass, effective spin, and merger rate to show that field binaries are unlikely to produce GW191109. Then, we also discuss why other dynamical channels (hierarchical systems and AGN disks) are unlikely to explain this event.

# 3.1. Isolated Binary Evolution

The isolated binary evolution channel for BBH formation involves two massive stars ( $\gtrsim 20\,M_\odot$ ) in a relatively close orbit. Typically, the more massive one leaves its main sequence first, expanding in radius and possibly donating mass to the companion when filling its Roche lobe. Eventually, the primary undergoes a supernova (SN) explosion or directly collapses to form a BH. After the secondary also leaves its main sequence and expands, the system can have a phase of either stable or unstable mass transfer. In the latter case, a common envelope may form (Paczynski 1976; van den Heuvel 1976; Tutukov & Yungelson 1993; Belczynski et al. 2002; Dominik et al. 2012; Stevenson et al. 2017; Giacobbo & Mapelli 2018). After the secondary also undergoes an SN explosion or direct collapse to a BH, a bound BBH is formed, which may merge in a Hubble time.

In our analysis, we model the formation of GW191109 through isolated binary evolution using the following simple assumptions.

- 1. The more massive star forms the more massive BH in the binary first, with no contribution to the final tilt of the orbital plane, as we assume that alignment of the BH spins and the binary orbital angular momentum occurred before the formation of the second BH.
- 2. The kick from the second SN is the primary contribution to the tilt of the orbital plane with respect to the BBH spin axes.
- 3. The natal kick imparted to the secondary BH at birth is isotropic.

With our methodology, we are able to conduct a controlled analysis of how different initial parameters affect the final distribution of tilts, thus avoiding all of the uncertainties associated with modeling the full formation process. Moreover, the component masses of GW191109 (particularly the primary) lie in the mass gap, which can be formed in isolated binaries only when considering the uncertain combined effect of the hydrogen-rich envelopes, dredge-ups, and  $^{12}\text{C}(\alpha, \gamma)^{16}\text{O}$  nuclear rates in massive stars (e.g., Farmer et al. 2020; Renzo et al. 2020; Costa et al. 2021). Concerning spins, we expect that the phases of mass transfer cause the alignment of the spin axes of the stars and BHs to the orbital angular momentum. As a result, the main contribution to the spin misalignment with respect to the orbital angular momentum (to eventually get a negative effective spin) is the natal kick imparted by an asymmetric SN explosion when forming the secondary BH.

To quantitatively assess the distributions of spin-orbit misalignment produced as a result of natal kicks, we compute

the tilt of the binary orbit by comparing pre- and post-SN energy and angular momentum (Hills 1983; Brandt & Podsiadlowski 1995; Kalogera 1996, 2000; Pijloo et al. 2012; Fragione et al. 2021). We consider a binary of masses  $m_{\rm BH,1}$  and  $m_2$ , semimajor axis a, and eccentricity e. The new orbital semimajor axis  $a_{\rm n}$ , eccentricity  $e_{\rm n}$ , and spin—orbit misalignment change as a result of an SN explosion of the secondary due to mass loss ( $\Delta m_2 = m_2 - m_{\rm BH,2}$ ), and the isotropic natal kick  $v_k$  on the newly born BH is imparted. Assuming that the SN takes place instantaneously, at a relative separation r and velocity v, the misalignment between the post- and pre-SN orbit is

$$\Delta \theta = \arccos\left(\frac{\boldsymbol{h} \cdot \boldsymbol{h}_{\mathrm{n}}}{h \ h_{\mathrm{n}}}\right),\tag{1}$$

where

$$|\mathbf{h}|^2 = |\mathbf{r} \times \mathbf{v}|^2 = G(m_{\text{BH},1} + m_2)a(1 - e)^2$$
 (2)

is the pre-SN angular momentum, and

$$|\mathbf{h}_n|^2 = |\mathbf{r} \times \mathbf{v}_n|^2 = G(m_{\text{BH},1} + m_{\text{BH},2})a_n(1 - e_n)^2$$
 (3)

is the post-SN angular momentum, with  $v_n = v + v_k$  being the new relative velocity.

Since we are modeling binary systems that result in a GW191109-like merger, we set the primary mass to be 65  $M_{\odot}$  and the post-SN secondary mass to be 47  $M_{\odot}$ , taking the medians of their respective parameter estimation distributions. For the remaining parameters, we test a range of initial conditions for a total of 96 different models.

- 1. Initial semimajor axis. We test both log-uniform and uniform distributions with ranges of  $10^{-2}$ – $10^{-1}$  and  $10^{-2}$ –1 au for a total of four distinct semimajor axis distributions.
- 2. Initial eccentricity. We take into account both uniform and thermal distributions for a total of two distinct eccentricity distributions.
- 3. Pre-SN mass of  $m_2$ . We consider three distinct pre-SN mass distributions for  $m_2$ . The first pre-SN mass distribution we test is a uniform distribution in the range  $47.5-57 M_{\odot}$ . The other two pre-SN mass distributions are simulated distributions generated using the Single Star Evolution (SSE) code with metallicities of 0.001 and 0.01 (Hurley et al. 2000). For the SSE simulations, we run a population of single stars to Hubble time and extract only stars with post-SN masses within the mass error range of the GW191109 secondary mass (34-62  $M_{\odot}$ ). Since it is unfeasible to obtain stars with an exact mass of 47  $M_{\odot}$ through SSE, we consider LVK's mass error range and assume that the mass loss experienced by these stars is representative of a 47  $M_{\odot}$  star. We show the SSEsimulated mass-loss distributions in Figures A1 and A2. We add these mass-loss values to the GW191109 secondary mass median value, 47  $M_{\odot}$ , to get the two SSE pre-SN mass distributions.
- 4. Kick velocity. We use a Maxwellian distribution,

$$p(v_{\rm kick}) \propto v_{\rm kick}^2 \exp\left(-\frac{v_{\rm kick}^2}{2\sigma^2}\right),$$
 (4)

with velocity dispersion  $\sigma$  to model the velocity kick imparted to the secondary BH at birth. Since  $\sigma$  is highly uncertain, we consider four different models. We use  $\sigma = 50$ , 100, and 265 km s<sup>-1</sup> for three of our models.

Table 1
Probability of Producing Systems with Tilt Greater than  $\pi/2$  after the Secondary SN Kicks

	Momentum Conservation	$\sigma = 50 \text{ km s}^{-1}$	$\sigma = 100 \text{ km s}^{-1}$	$\sigma = 265 \text{ km s}^-$
Uniform mass loss				
a: log-uniform (0.1 au), e: uniform	0*	$5.9 \times 10^{-4}$	$2.3 \times 10^{-3}$	$1.5 \times 10^{-2}$
a: log-uniform (0.1 au), e: thermal	$2 \times 10^{-5*}$	$1.2 \times 10^{-3}$	$4.5 \times 10^{-3}$	$2.7 \times 10^{-2}$
a: uniform (0.1 au), e: uniform	$0^*$	$8.4 \times 10^{-4}$	$3.3 \times 10^{-3}$	$2.1 \times 10^{-2}$
a: uniform (0.1 au), e: thermal	$2 \times 10^{-5*}$	$1.9 \times 10^{-3}$	$6.6 \times 10^{-3}$	$3.8 \times 10^{-2}$
a: log-uniform (1 au), e: uniform	$7 \times 10^{-5}$	$3.8 \times 10^{-3}$	$1.2 \times 10^{-2}$	$4.5 \times 10^{-2}$
a: log-uniform (1 au), e: thermal	$1.1 \times 10^{-4}$	$6.5 \times 10^{-3}$	$2.2 \times 10^{-2}$	$6.8 \times 10^{-2}$
a: uniform (1 au), e: uniform	$3.2 \times 10^{-4}$	$1.5 \times 10^{-2}$	$4.0 \times 10^{-2}$	0.12
a: uniform (1 au), e: thermal	$4.4 \times 10^{-4}$	$2.2 \times 10^{-2}$	$6.3 \times 10^{-2}$	0.15
SSE mass loss (0.001)				
a: log-uniform (0.1 au), e: uniform	$2 \times 10^{-5*}$	$6.1 \times 10^{-4}$	$2.5 \times 10^{-3}$	$1.6 \times 10^{-2}$
a: log-uniform (0.1 au), e: thermal	$0^*$	$1.2 \times 10^{-3}$	$5.0 \times 10^{-3}$	$3.0 \times 10^{-2}$
a: uniform (0.1 au), e: uniform	$2 \times 10^{-5*}$	$8.8 \times 10^{-4}$	$3.6 \times 10^{-3}$	$2.3 \times 10^{-2}$
a: uniform (0.1 au), e: thermal	$4 \times 10^{-5*}$	$1.8 \times 10^{-3}$	$6.4 \times 10^{-3}$	$4.2 \times 10^{-2}$
a: log-uniform (1 au), e: uniform	$4 \times 10^{-5}$	$6.4 \times 10^{-4}$	$2.5 \times 10^{-3}$	$1.6 \times 10^{-2}$
a: log-uniform (1 au), e: thermal	$2 \times 10^{-5}$	$1.1 \times 10^{-3}$	$4.5 \times 10^{-3}$	$3.0 \times 10^{-2}$
a: uniform (1 au), e: uniform	$2.9 \times 10^{-4}$	$1.4 \times 10^{-2}$	$4.1 \times 10^{-2}$	0.13
a: uniform (1 au), e: thermal	$7.0 \times 10^{-4}$	$2.2 \times 10^{-2}$	$6.4 \times 10^{-2}$	0.16
SSE mass loss (0.01)				
a: log-uniform (0.1 au), e: uniform	$0^*$	$6.7 \times 10^{-4}$	$2.2 \times 10^{-3}$	$1.5 \times 10^{-2}$
a: log-uniform (0.1 au), e: thermal	$10^{-5*}$	$1.2 \times 10^{-3}$	$4.5 \times 10^{-3}$	$2.8 \times 10^{-2}$
a: uniform (0.1 au), e: uniform	$2 \times 10^{-5*}$	$8.5 \times 10^{-4}$	$3.1 \times 10^{-3}$	$2.1\times10^{-2}$
a: uniform (0.1 au), e: thermal	$2 \times 10^{-5*}$	$1.7 \times 10^{-3}$	$6.0 \times 10^{-3}$	$3.8 \times 10^{-2}$
a: log-uniform (1 au), e: uniform	$10^{-5}$	$5.1 \times 10^{-4}$	$2.1 \times 10^{-3}$	$1.5 \times 10^{-2}$
a: log-uniform (1 au), e: thermal	$10^{-5}$	$1.2 \times 10^{-3}$	$4.2 \times 10^{-3}$	$2.8 \times 10^{-2}$
a: uniform (1 au), e: uniform	$2.5 \times 10^{-4}$	$1.3 \times 10^{-2}$	$4.0 \times 10^{-2}$	0.12
a: uniform (1 au), e: thermal	$4.4 \times 10^{-4}$	$2.2 \times 10^{-2}$	$6.4 \times 10^{-2}$	0.16

Note. Note that the (0.1 au) or (1 au) in each model is the upper bound for the semimajor axis range. Values with an asterisk indicate the models that are more physically motivated.

Note that  $\sigma = 265 \text{ km s}^{-1}$  is the typical kick expected for neutron stars as found by Hobbs et al. (2005), while  $\sigma = 100 \text{ km s}^{-1}$  in the analysis of Arzoumanian et al. (2002). For the fourth model, we adopt natal kicks from Equation (4) as for neutron stars but with  $\sigma$  scaled by linear momentum conservation as follows (Repetto et al. 2012; Janka 2013):

$$v_{\rm BH} = \frac{\langle m_{\rm NS} \rangle}{m_{\rm BH}} v_{\rm NS},\tag{5}$$

where  $v_{\rm BH}$  is the natal kick on a BH with mass  $m_{\rm BH}$ ,  $\langle m_{\rm NS} \rangle \approx 1.3~M_{\odot}$  is the average mass of neutron stars, and  $v_{\rm NS}$  is randomly drawn from the Maxwellian distribution with  $\sigma = 265~{\rm km~s^{-1}}$ . Here we fix  $m_{\rm BH}$  to 47  $M_{\odot}$ , the median mass of the secondary BH in GW191109. We label this model in Table 1 "Momentum Conservation." We note that more recently, non-Maxwellian distributions have been used in the literature (Kapil et al. 2023), but we do not test these distributions in our modeling.

For each combination of parameter distributions, we simulate  $10^5$  binaries, for a total of 9.6 million binaries.

Our results primarily focus on the final tilt after the second SN. In order to have a negative  $\chi_{\rm eff}$ , the natal kick imparted to the secondary has to be strong enough to tilt the orbital angular momentum more than  $\pi/2$  with respect to its initial orientation. In Figure 2, we show the cumulative distribution of the final tilts for binaries, with an initial semimajor axis distribution following a log-uniform distribution in the range  $10^{-2}$ - $10^{-1}$  au, an initial uniform eccentricity distribution, and an SSE-

simulated pre-SN mass distribution with metallicity 0.01. The models in Figure 2 clearly demonstrate that it is unlikely to tilt binaries above  $\pi/2$ , and a direct correlation exists between higher velocity kicks and the fraction of binaries experiencing greater tilts. Specifically, no binaries experienced tilts greater than  $\pi/2$  when the velocity kick distribution followed momentum conservation, and  $6.7 \times 10^{-4}$ ,  $2.16 \times 10^{-3}$ , and  $1.535 \times 10^{-2}$  of the  $10^5$  binaries experienced tilts greater than  $\pi/2$  for Maxwellian velocity kick distributions with  $\sigma=50$ , 100, and  $265 \text{ km s}^{-1}$ , respectively.

The results for all 96 models are summarized in Table 1. We place an asterisk next to the values corresponding to models that are more likely to be representative of a population of merging BBHs. One of the factors that we consider is whether or not the BBHs can merge in a Hubble time to be observed today, given the merger timescale (Peters 1964)

$$T_{\rm GW} \approx 13 {\rm Gyr} \left( \frac{2 \times 10^3 \, M_{\odot}^3}{m_{\rm BH,1} m_{\rm BH,2} (m_{\rm BH,1} + m_{\rm BH,2})} \right) \times \left( \frac{a_n}{0.095 {\rm au}} \right)^4 (1 - e_n^2)^{7/2}.$$
 (6)

This equation places a limit on how large the semimajor axis can be in order for a BBH to merge in a Hubble time. Specifically, given  $m_{\rm BH,1}$  and  $m_{\rm BH,1}$  as 65 and 47  $M_{\odot}$ , respectively, a semimajor axis of 1 au would require at least a 0.84 eccentricity for the merger timescale to be less than a Hubble time. On the other hand, a semimajor axis of 0.1 au would allow for the full range of eccentricities. Thus, a uniform

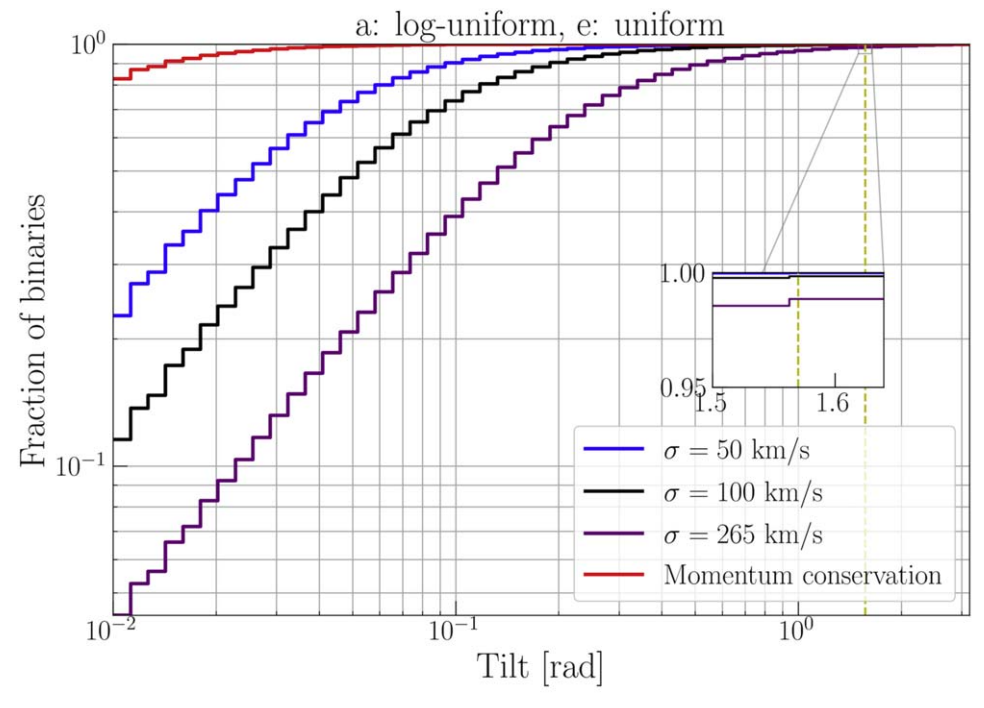


Figure 2. Cumulative distribution of the final tilts for binaries with the following initial conditions: the mass-loss distribution is simulated by SSE with initial metallicities of 0.01 (see Figure A2), the initial semimajor axis distribution is log-uniform with a range of  $10^{-2}$ – $10^{-1}$  au, and the initial eccentricity distribution is uniform. Different colors show different kick velocity distributions:  $\sigma = 50$  (blue), 100 (black), 265 (purple), and 265 km s<sup>-1</sup> scaled by momentum conservation (red). The dotted yellow line marks  $\pi/2$ , the tilt angle at which the spin of the post-SN mass would be antialigned with the orbital angular momentum, possibly producing a negative  $\chi_{\rm eff}$ .

or log-uniform semimajor distribution ranging from 0.01 to 0.1 au is more likely to be representative of a population of merging BBHs than that of the range 0.01-1 au. For completeness, we show all of these models in Table 1, but we place an asterisk on the values with an upper bound of 0.1 au for the semimajor axis distribution. Another factor to consider as to what more likely represents a population of merging BBHs is the velocity kick distribution. A Maxwellian distribution with a  $\sigma$  value of 265 km s<sup>-1</sup> is the expected velocity kick distribution for neutron stars but is very unlikely to be the case for much more massive BHs, due to momentum conservation (Belczynski et al. 2008). Thus, we add an asterisk to the numbers in Table 1 that assume a momentum conservation velocity kick distribution. Looking at the values with asterisks in Table 1, we find that, at most, only 0.004% of the isolated binaries can be tilted enough such that negative effective inspiral spin is produced.

Due to the improbable chance of creating a binary with both a negative  $\chi_{\rm eff}$  and BH component masses in the mass gap (e.g., Belczynski et al. 2020; Farmer et al. 2020; Renzo et al. 2020; Costa et al. 2021), the rates for this formation channel would therefore be too low to explain GW191109. Thus, we conclude that isolated binary evolution is very unlikely to produce GW191109-like events.

# 3.2. Dynamics in Dense Star Clusters

Merging BBHs can be assembled dynamically in dense star clusters. Here BHs quickly segregate to the center through dynamical friction (Chandrasekhar 1943; Spitzer 1987) and interact with each other to form binaries. If the binary is hard, subsequent three- and four-body encounters with other BHs

further harden the binary by extracting orbital energy (Heggie 1975), which can eventually merge (e.g., McMillan et al. 1991; Hut et al. 1992; Portegies Zwart & McMillan 2000; Rodriguez et al. 2016; Fragione et al. 2018; Samsing et al. 2018; Banerjee et al. 2020).

An interesting possibility for BBH mergers formed through dynamical interactions is that the merger remnant can be retained in the parent cluster whenever the relativistic recoil kick imparted as a result of asymmetric emission of GWs is smaller than the cluster escape speed (e.g., Lousto et al. 2010, 2012). The retained BH, which is now a secondgeneration (2G) BH, can be dynamically processed again to form a new BBH system that eventually merges. Highergeneration mergers account for ~10% of mergers from globular clusters, with this fraction increasing for denser environments such as nuclear star clusters (e.g., Antonini et al. 2019; Rodriguez et al. 2019; Mapelli et al. 2021; Fragione et al. 2022a, 2022b). From the second LIGO-Virgo GW Transient Catalog, Kimball et al. (2021) found that the catalog contains at least one 2G merger with 99% credibility and lists five BBH mergers with high odds of involving at least one 2G BH.

In Figure 3, we show the component masses of the merging BBH extracted from the public globular cluster models of Kremer et al. (2020). Out of 148 globular cluster models, we find that there are 169 1G–2G and 24 2G–2G BBHs that have primary and secondary masses consistent with the 90% confidence interval mass ranges of GW191109 (The LIGO Scientific Collaboration et al. 2021). Note that some of the 1G BHs have masses well within the mass gap, since they originate from the collapse of very massive stars born as a result of repeated stellar mergers (González et al. 2021). Therefore, 1G–2G and 2G–2G BBHs dynamically formed in dense star clusters can easily produce the masses of GW191109-like

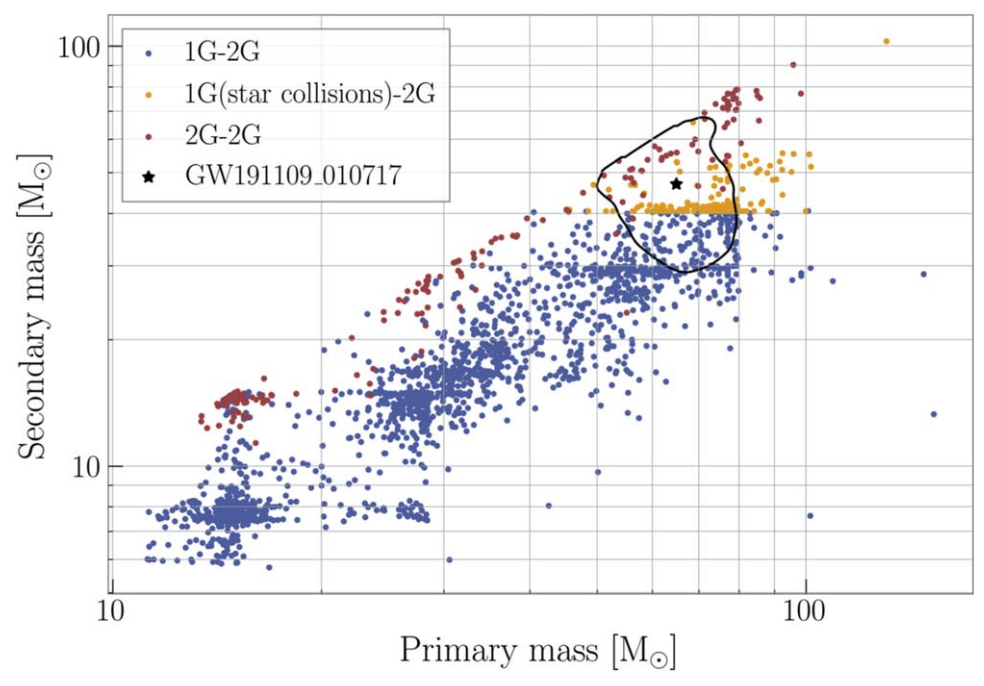


**Figure 3.** Primary and secondary mass of 1G–2G and 2G–2G BBHs from 148 simulated globular clusters in the models of Kremer et al. (2020). For 1G–2G mergers, we distinguish between 1G BHs born as a result of the collapse of massive stars (blue points) and 1G BHs formed via star collisions (yellow points). We label GW191109's median component masses with a black star, with the contour corresponding to its 90% confidence region in mass space.

events despite lying in the pair-instability mass gap, unlike isolated binaries.

For dynamically assembled BBHs, the population of BH spins relative to the orbital angular momentum axis is isotropic as a result of the few-body encounters that catalyze the merger of BBHs. We assume that 1G BHs are born with negligible spin (Qin et al. 2018; Fuller & Ma 2019) and 2G BHs have spins of about 0.7 (e.g., Buonanno et al. 2008; Tichy & Marronetti 2008). Combining the isotropically distributed spin directions with the component masses of GW191109, we get  $\chi_{\rm eff}$  distributions for both 1G–2G and 2G–2G BBHs, as shown in Figure 4. Since the distributions are symmetric around zero, with the 1G-2G distribution uniformly distributed between -0.41 and 0.41 and the 2G-2G distribution isotropically distributed about zero between -0.70 and 0.70, negative values of  $\chi_{\rm eff}$  are as likely as positive values. Under the assumption that 1G BHs are born with negligible spin, the median  $\chi_{\rm eff}$ value of GW191109 of -0.29 can be easily accounted for with dynamically assembled BBHs as long as one of the components is a 2G BH.

Finally, we use the number of merging BBHs consistent with GW191109 to compute the rates of GW191109-like events,

$$R = \frac{N\rho_{\rm GC}}{\tau_{\rm H}},\tag{7}$$

where N is the number of BBHs in the GW191109 mass range per globular cluster,  $\rho_{GC}$  is the density of globular clusters in the Universe, and  $\tau_{H}$  is the Hubble time. We extract N from Figure 3 by taking the number of simulated 1G–2G and 2G–2G events with masses within the GW191109 90% confidence interval range and dividing it by the total number of simulated globular clusters, which is 169/148 and 24/148, respectively. We assume a value of  $0.77~{\rm Mpc}^{-3}$  for  $\rho_{GC}$  with an optimistic value of  $2.31~{\rm Mpc}^{-3}$  and pessimistic value of  $0.32~{\rm Mpc}^{-3}$  using the calculations from Rodriguez et al. (2015). In Figure 5,

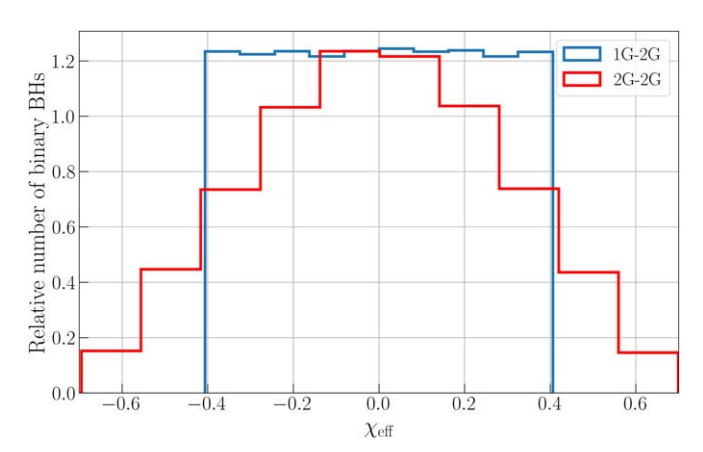


**Figure 4.** Distribution of effective spin for 1G–2G and 2G–2G BBHs for component masses consistent with GW191109 and assuming nonspinning 1G BHs. Both distributions are symmetric around zero, with a nonnegligible likelihood of reproducing negative  $\chi_{\rm eff}$  values.

we indicate the rate calculation assuming  $\rho_{\rm GC}=0.77\,{\rm Mpc^{-3}}$  with the vertical green dotted line, and the shaded region accounts for the range of calculated rates bounded by the optimistic and pessimistic values for  $\rho_{\rm GC}$ . Assuming  $\rho_{\rm GC}=0.77\,{\rm Mpc^{-3}}$ , we get an approximate rate for 1G–2G events of 0.064 Gpc<sup>-3</sup> yr<sup>-1</sup> and 2G–2G events of 0.0090 Gpc<sup>-3</sup> yr<sup>-1</sup>, leading to a total rate of 0.073 Gpc<sup>-3</sup> yr<sup>-1</sup> for 1G–2G or 2G–2G events having masses in the GW191109 90% confidence interval range. For an optimistic value of  $\rho_{\rm GC}=2.31\,{\rm Mpc^{-3}}$ , that total rate rises to 0.218 Gpc<sup>-3</sup> yr<sup>-1</sup>, and for a pessimistic value of  $\rho_{\rm GC}=0.32\,{\rm Mpc^{-3}}$ , that total rate decreases to 0.030 Gpc<sup>-3</sup> yr<sup>-1</sup>.

We then compare our estimate to the expected number of GW191109-like mergers given one detection by the LIGO-Virgo detector network. Following the method described in Kim et al. (2003), we calculate this rate assuming one

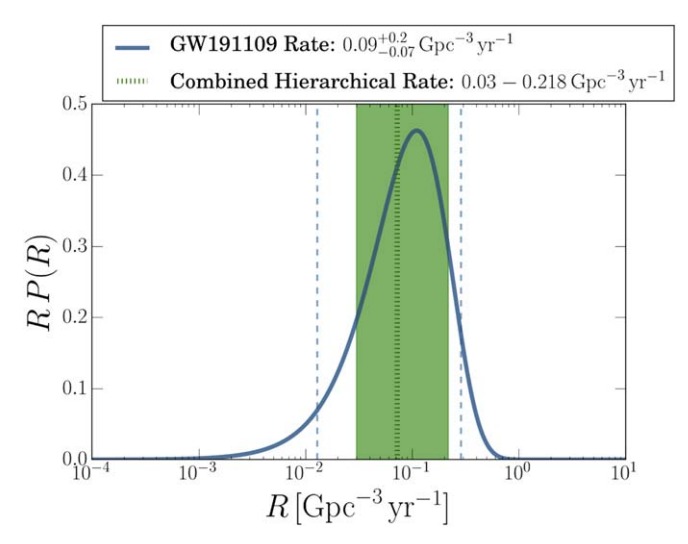


**Figure 5.** In solid blue, we plot the posterior over the rate of GW191109-like mergers assuming one Poisson-distributed count from a population drawn from the public parameter estimation samples. The dashed blue lines indicate the 90% confidence interval. The dotted green line marks the combined 1G–2G and 2G–2G merger rate, assuming  $\rho_{\rm GC}=0.77~{\rm Mpc}^{-3}$ , and the shaded green region marks the range of rates bounded by assuming  $\rho_{\rm GC}=0.32$  and  $2.31~{\rm Mpc}^{-3}$ .

Poisson-distributed count from a BBH population with masses and spins drawn from the publicly available parameter estimation samples for GW191109 (The LIGO Scientific Collaboration et al. 2021). We calculate the network sensitivity to this population across O1, O2, and O3 using a combined signal-to-noise ratio of 10 as a detection threshold. Using an  $R^{-1/2}$  Jeffrey's prior, we find a GW191109-like merger rate of  $R_{191109} = 0.09^{+0.2}_{-0.07}$  Gpc<sup>-3</sup> yr<sup>-1</sup> (90% confidence interval) and plot the rate posterior in Figure 5. Here we see that the simulated combined hierarchical rate lies well within the rate distribution of detecting a GW191109-like merger.

In summary, BBHs assembled in dense star clusters can explain the mass, effective spin, and rate of GW191109, unlike isolated binary evolution. Also note that our interpretation of GW191109 as having a dynamical origin is consistent with the findings in Romero-Shaw et al. (2022). In this study, they used a reweighting method (Payne et al. 2019; Romero-Shaw et al. 2019) to calculate the eccentricity posterior probability distribution and found 72.19% of its posterior support at an eccentricity above 0.05 and 62.63% above 0.1. This likely nonzero orbital eccentricity also points toward a dynamical origin of GW191109, consistent with our results.

#### 3.3. Other Channels

Another astrophysical scenario to consider for the possible formation of GW191109-like events is the AGN channel (e.g., Bartos et al. 2017; Tagawa et al. 2020a). The spin evolution of stellar-mass BHs in AGN disks was studied by Tagawa et al. (2020b). Through their semianalytical simulations, they found that while gas accretion enhances the effective spin toward more positive values, hard binary–single interactions in the disks may reduce it. Therefore, the more efficient the radial migration of BHs to inner, densely populated regions of the AGN disk is, the more symmetric around zero the distribution of the effective spin of merging BBHs is. However, if this migration is inefficient, then the  $\chi_{\rm eff}$  values would be skewed toward higher values. Tagawa et al. (2020b) found that BBH

mergers with component masses in the mass gap can be reproduced in the AGN channel, but their rates are highly uncertain. Considering the effective inspiral spin, masses, and rates, we cannot confidently say that GW191109 is likely to be formed via the AGN disk channel.

Hierarchical triple systems have been extensively studied in the literature (e.g., Antonini & Perets 2012; Hoang et al. 2018; Hamers et al. 2021). Using population synthesis of triple stars that form a BH triplet, Martinez et al. (2022) found that the distribution of effective spins for merging BBHs is likely symmetric around zero as a result of the Lidov–Kozai oscillations. Therefore, hierarchical systems can produce mergers with a negative value of  $\chi_{\rm eff}$ . However, this channel is unlikely to produce mass gap BBHs for the same reasons isolated binaries cannot; that is, the masses of the component BHs are limited by the pair-instability physics. Finally, Martinez et al. (2022) found that although highly uncertain, the hierarchical triple rates are estimated to possibly account for only a fraction of the observed BBH rates, which renders this scenario unlikely for GW191109-like events.

Because these other channels are unlikely to be the origin of GW191109-like events, we argue that dynamical assembly in dense star clusters is the most likely formation channel for GW191109.

### 4. Conclusions and Discussion

In this paper, we have demonstrated that GW191109 is unlikely to originate from isolated binary evolution based on its negative effective inspiral spin, masses, and inferred rate. Other channels, such as hierarchical systems and AGN disks, are also unlikely to explain GW191109. Combined with the possibility of nonzero eccentricity (Romero-Shaw et al. 2022), all the evidence points toward a dynamical origin for this source.

Furthermore, this result can be extended to binary systems of any mass with some uncertainties. Kalogera (2000) applied a similar prescription for BBH binaries, testing much lower masses in the 5–20  $M_{\odot}$  range, and found that even by assuming a Maxwellian distribution with  $\sigma = 200 \text{ km s}^{-1}$  for the velocity kicks, it is extremely unlikely for isolated binary evolution to tilt a BH over  $\pi/2$  to contribute to a negative effective inspiral spin. We have reproduced similar results using our prescriptions for the different models with the BBH masses attained from GW200225, 19.3 and  $14 M_{\odot}$ . This GW event, as shown in Figure 1, also has a very likely negative effective inspiral spin. For the models involving a semimajor axis distribution with an upper bound of 0.1 au and velocity kicks following momentum conservation, no more than 0.09% of all binaries can be tilted over  $\pi/2$  to produce a negative effective inspiral spin, demonstrating that, even regardless of mass, it is extremely unlikely for isolated binary evolution to produce a negative effective inspiral spin. We note that a recent alternative theory for isolated binary evolution producing negative effective inspiral spins was suggested by Tauris (2022) as a result of the spin-axis tossing of BHs during their formation process in the core collapse of a massive star.

To study isolated binary evolution in our simulations, we have modeled how a binary system is affected after the second SN occurs in the system. It is possible that the first SN could also help tilt the binary system, increasing the total tilt of the BBHs' spins with respect to the angular momentum vector. While this is true, this contribution to the tilt will likely be smaller, as the binary was more massive during the first SN,

making it more difficult to tilt the orbital plane. Given that the second SN is already unlikely to tilt the binary systems over  $\pi/2$ , the kick the BH experiences by the first SN would be even more unlikely to contribute to such a tilt.

Finally, it is worth noting that in LIGO/Virgo's O3 run, approximately 20% of the signals experienced glitches. The official LVK release data took this effect into account by modeling the glitch in their inference estimation. In the case of GW191109, the glitch was experienced by the Livingston data between 20 and 40 Hz. If these data are entirely removed from the inference, Davis et al. (2022) found that the  $\chi_{\rm eff}$  distribution does not peak strongly in the negative values anymore. While this information does not imply that a conclusion about the true  $\chi_{\rm eff}$  distribution can be drawn, it does emphasize the uncertainties for the measurement. Additionally, we note that the LVK data analysis pipeline assumes a prior of isotropic spins for all of the GW events (The LIGO Scientific Collaboration et al. 2021), which may affect the posterior  $\chi_{\rm eff}$  distribution. Even if the information on the  $\chi_{\rm eff}$  of GW191109 is excluded from the analysis of its origin, its masses and rates still strongly point toward a dynamical origin.

With the LVK O4 run coming up in the next year, the population of BBHs will increase to hundreds of events, with the potential of providing better constraints on possible formation channels. Discovering BBHs with masses in the pair-instability mass gap, unequal mass ratios, and negative  $\chi_{\rm eff}$ , and inferred properties of nonzero orbital eccentricity and merger rates, will be good indicators of alternative formation channels from standard isolated binary evolution, such as dynamical origins. Thus, it will be important to place an emphasis on the analysis of these properties in future observations.

### Acknowledgments

We thank Fred Rasio, Salvatore Vitale, and Katerina Chatziioannou for useful comments on an earlier version of the manuscript. G.F. acknowledges support from NASA grant 80NSSC21K1722. C.K. is grateful for support from the Riedel Family Fellowship in Data Science in CIERA. V.K. was partially supported through a CIFAR Senior Fellowship and by Northwestern University, through the Daniel I. Linzer Distinguished University Professorship fund.

# Appendix Relative Mass-loss Distributions of SSE Simulations

In this appendix, we show the relative mass-loss distributions generated from SSE as explained in Section 3. We simulate the evolution of 10<sup>5</sup> single stars using SSE and plot the mass losses experienced from the SNe of those stars that have a post-SN mass that is within the error bar range of the GW191109 secondary mass. Figures A1 and A2 show the relative distributions of mass loss given initial star metallicities of 0.001 and 0.01, respectively.

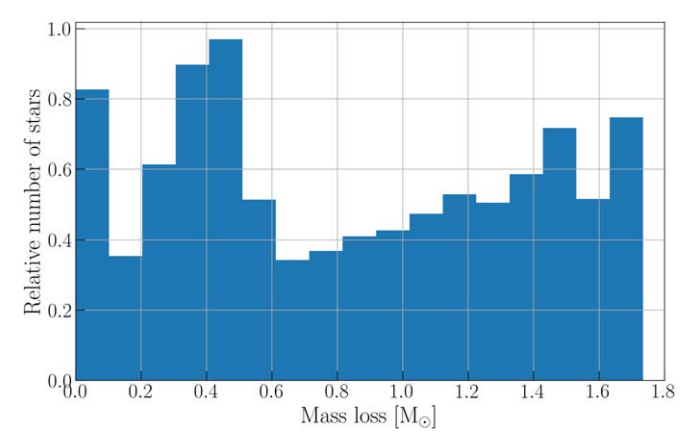


**Figure A1.** Relative mass-loss distribution for an SSE-simulated population of single stars with initial metallicities of 0.001 and final masses within the error bar range of the GW191109 secondary mass.

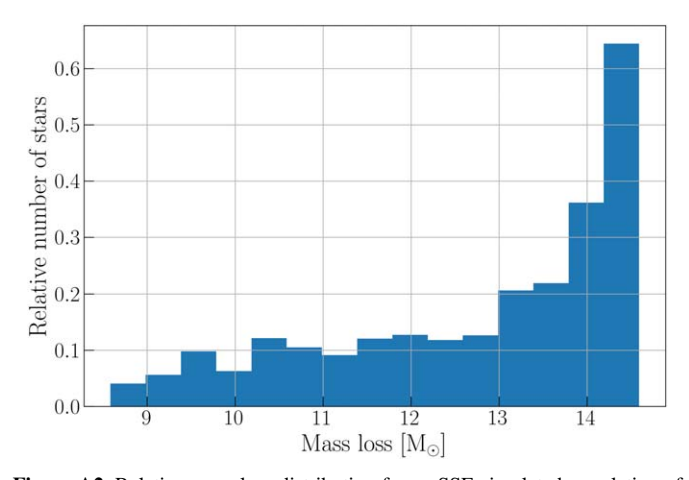


**Figure A2.** Relative mass-loss distribution for an SSE-simulated population of single stars with initial metallicities of 0.01 and final masses within the error bar range of the GW191109 secondary mass.

# **ORCID iDs**

Rachel C. Zhang https://orcid.org/0000-0002-2905-9239 Giacomo Fragione https://orcid.org/0000-0002-7330-027X Chase Kimball https://orcid.org/0000-0001-9879-6884 Vicky Kalogera https://orcid.org/0000-0001-9236-5469

# References

Abbott, R., Abbott, T.D., Abraham, S., et al. 2021a, ApJL, 913, L7
Abbott, R., Abbott, T.D., Abraham, S., et al. 2021b, PhRvD, 103, 122002
Abbott, R., Abbott, T. D., Abraham, S., et al. 2021c, PhRvX, 11, 021053
Antonini, F., Gieles, M., & Gualandris, A. 2019, MNRAS, 486, 5008
Antonini, F., & Perets, H. B. 2012, ApJ, 757, 27
Antonini, F., & Rasio, F. A. 2016, ApJ, 831, 187
Arzoumanian, Z., Chernoff, D. F., & Cordes, J. M. 2002, ApJ, 568, 289
Askar, A., Szkudlarek, M., Gondek-Rosińska, D., Giersz, M., & Bulik, T. 2017, MNRAS, 464, L36
Banerjee, S. 2017, MNRAS, 467, 524

Banerjee, S. 2018a, MNRAS, 473, 909

```
Banerjee, S. 2018b, MNRAS, 481, 5123
Banerjee, S., Belczynski, K., Fryer, C. L., et al. 2020, A&A, 639, A41
Bartos, I., Kocsis, B., Haiman, Z., & Márka, S. 2017, ApJ, 835, 165
Bavera, S. S., Fragos, T., Zevin, M., et al. 2021, A&A, 647, A153
Belczynski, K., Holz, D. E., Bulik, T., & O'Shaughnessy, R. 2016a, Natur,
Belczynski, K., Kalogera, V., & Bulik, T. 2002, ApJ, 572, 407
Belczynski, K., Kalogera, V., Rasio, F. A., et al. 2008, ApJS, 174, 223
Belczynski, K., Klencki, J., Fields, C. E., et al. 2020, A&A, 636, A104
Belczynski, K., Repetto, S., Holz, D. E., et al. 2016b, ApJ, 819, 108
Bond, J. R., Arnett, W. D., & Carr, B. J. 1984, ApJ, 280, 825
Brandt, N., & Podsiadlowski, P. 1995, MNRAS, 274, 461
Buonanno, A., Kidder, L. E., & Lehner, L. 2008, PhRvD, 77, 026004
Chandrasekhar, S. 1943, ApJ, 97, 255
Costa, G., Bressan, A., Mapelli, M., et al. 2021, MNRAS, 501, 4514
Davis, D., Littenberg, T. B., Romero-Shaw, I. M., et al. 2022, CQGra, 39, 245013
de Mink, S. E., Cantiello, M., Langer, N., et al. 2009, A&A, 497, 243
de Mink, S. E., & Mandel, I. 2016, MNRAS, 460, 3545
Di Carlo, U. N., Giacobbo, N., Mapelli, M., et al. 2019, MNRAS, 487, 2947
Dominik, M., Belczynski, K., Fryer, C., et al. 2012, ApJ, 759, 52
Dominik, M., Belczynski, K., Fryer, C., et al. 2013, ApJ, 779, 72
eLISA Consortium, Amaro Seoane, P., Aoudia, S., et al. 2013,
   arXiv:1305.5720
Farmer, R., Renzo, M., de Mink, S. E., et al. 2020, ApJL, 902, L36
Farmer, R., Renzo, M., de Mink, S. E., Marchant, P., & Justham, S. 2019, ApJ,
   887, 53
Fowler, W. A., & Hoyle, F. 1964, ApJS, 9, 201
Fragione, G., & Banerjee, S. 2021, ApJL, 913, L29
Fragione, G., Ginsburg, I., & Kocsis, B. 2018, ApJ, 856, 92
Fragione, G., Grishin, E., Leigh, N. W. C., et al. 2019, MNRAS, 488, 47
Fragione, G., & Kocsis, B. 2018, PhRvL, 121, 161103
Fragione, G., Kocsis, B., Rasio, F. A., & Silk, J. 2022a, ApJ, 927, 231
Fragione, G., Loeb, A., Kocsis, B., & Rasio, F. A. 2022b, ApJ, 933, 170
Fragione, G., Loeb, A., & Rasio, F. A. 2020, ApJL, 902, L26
Fragione, G., Loeb, A., & Rasio, F. A. 2021, ApJL, 918, L38
Fragione, G., & Silk, J. 2020, MNRAS, 498, 4591
Fuller, J., & Ma, L. 2019, ApJL, 881, L1
Galaudage, S., Talbot, C., Nagar, T., et al. 2021, ApJL, 921, L15
Gayathri, V., Healy, J., Lange, J., et al. 2022, NatAs, 6, 344
Gerosa, D., & Berti, E. 2017, PhRvD, 95, 124046
Giacobbo, N., & Mapelli, M. 2018, MNRAS, 480, 2011
González, E., Kremer, K., Chatterjee, S., et al. 2021, ApJL, 908, L29
Hamers, A. S., Fragione, G., Neunteufel, P., & Kocsis, B. 2021, MNRAS,
  506, 5345
Heger, A., & Woosley, S. E. 2002, ApJ, 567, 532
Heggie, D. C. 1975, MNRAS, 173, 729
Hills, J. G. 1983, ApJ, 267, 322
Hoang, B.-M., Naoz, S., Kocsis, B., et al. 2018, ApJ, 856, 140
Hobbs, G., Lorimer, D. R., Lyne, A. G., & Kramer, M. 2005, MNRAS,
  360, 974
Hoy, C., & Raymond, V. 2021, SoftX, 15, 100765
Hurley, J. R., Pols, O. R., & Tout, C. A. 2000, MNRAS, 315, 543
Hut, P., McMillan, S., Goodman, J., et al. 1992, PASP, 104, 981
Janka, H.-T. 2013, MNRAS, 434, 1355
Kalogera, V. 1996, ApJ, 471, 352
Kalogera, V. 2000, ApJ, 541, 319
Kalogera, V., Belczynski, K., Kim, C., O'Shaughnessy, R., & Willems, B.
  2007, PhR, 442, 75
Kapil, V., Mandel, I., Berti, E., & Müller, B. 2023, MNRAS, 519, 5893
Kim, C., Kalogera, V., & Lorimer, D. R. 2003, ApJ, 584, 985
Kimball, C., Talbot, C., Berry, C. P. L., et al. 2021, ApJL, 915, L35
Kremer, K., Ye, C. S., Rui, N. Z., et al. 2020, ApJS, 247, 48
Lousto, C. O., Campanelli, M., Zlochower, Y., & Nakano, H. 2010, CQGra,
```

27, 114006

```
Lousto, C. O., Zlochower, Y., Dotti, M., & Volonteri, M. 2012, PhRvD, 85,
Maggiore, M., Van Den Broeck, C., Bartolo, N., et al. 2020, JCAP, 2020, 050
Mandel, I., & de Mink, S. E. 2016, MNRAS, 458, 2634
Mapelli, M., Dall'Amico, M., Bouffanais, Y., et al. 2021, MNRAS, 505, 339
Marchant, P., Langer, N., Podsiadlowski, P., Tauris, T. M., & Moriya, T. J.
  2016, A&A, 588, A50
Martinez, M. A. S., Fragione, G., Kremer, K., et al. 2020, ApJ, 903, 67
Martinez, M. A. S., Rodriguez, C. L., & Fragione, G. 2022, ApJ, 937, 78
McMillan, S., Hut, P., & Makino, J. 1991, ApJ, 372, 111
Miller, M. C., & Hamilton, D. P. 2002, ApJ, 576, 894
Neijssel, C. J., Vigna-Gómez, A., Stevenson, S., et al. 2019, MNRAS,
  490, 3740
Paczynski, B. 1976, in IAU Symp. 73, Structure and Evolution of Close Binary
  Systems, ed. P. Eggleton, S. Mitton, & J. Whelan (Dordrecht: D. Reidel), 75
Payne, E., Talbot, C., & Thrane, E. 2019, PhRvD, 100, 123017
Peters, P. C. 1964, PhRv, 136, 1224
Pijloo, J. T., Caputo, D. P., & Portegies Zwart, S. F. 2012, MNRAS,
  424, 2914
Portegies Zwart, S. F., & McMillan, S. L. W. 2000, ApJL, 528, L17
Postnov, K. A., & Yungelson, L. R. 2014, LRR, 17, 3
Qin, Y., Fragos, T., Meynet, G., et al. 2018, A&A, 616, A28
Reitze, D., Adhikari, R. X., Ballmer, S., et al. 2019, BAAS, 51, 35
Renzo, M., Farmer, R. J., Justham, S., et al. 2020, MNRAS, 493, 4333
Repetto, S., Davies, M. B., & Sigurdsson, S. 2012, MNRAS, 425, 2799
Rodriguez, C. L., Amaro-Seoane, P., Chatterjee, S., & Rasio, F. A. 2018,
  PhRvL, 120, 151101
Rodriguez, C. L., Chatterjee, S., & Rasio, F. A. 2016, PhRvD, 93, 084029
Rodriguez, C. L., Kremer, K., Grudić, M. Y., Hafen, Z., et al. 2020, ApJL,
  896. L10
Rodriguez, C. L., Morscher, M., Pattabiraman, B., et al. 2015, PhRvL, 115,
  051101
Rodriguez, C. L., Zevin, M., Amaro-Seoane, P., et al. 2019, PhRvD, 100,
Romero-Shaw, I. M., Lasky, P. D., & Thrane, E. 2019, MNRAS, 490, 5210
Romero-Shaw, I. M., Lasky, P. D., & Thrane, E. 2022, ApJ, 940, 171
Roulet, J., Chia, H. S., Olsen, S., et al. 2021, PhRvD, 104, 083010
Samsing, J. 2018, PhRvD, 97, 103014
Samsing, J., & D'Orazio, D. J. 2018, MNRAS, 481, 5445
Samsing, J., MacLeod, M., & Ramirez-Ruiz, E. 2018, ApJ, 853, 140
Spera, M., Mapelli, M., Giacobbo, N., et al. 2019, MNRAS, 485, 889
Spitzer, L. 1987, Dynamical Evolution of Globular Clusters (Princeton, NJ:
  Princeton Univ. Press)
Stevenson, S., Vigna-Gómez, A., Mandel, I., et al. 2017, NatCo, 8, 14906
Su, Y., Liu, B., & Lai, D. 2021, MNRAS, 505, 3681
Tagawa, H., Haiman, Z., Bartos, I., & Kocsis, B. 2020a, ApJ, 899, 26
Tagawa, H., Haiman, Z., & Kocsis, B. 2020b, ApJ, 898, 25
Tagawa, H., Haiman, Z., & Kocsis, B. 2020c, ApJ, 892, 36
Tagawa, H., Saitoh, T. R., & Kocsis, B. 2018, PhRvL, 120, 261101
Tauris, T. M. 2022, ApJ, 938, 66
The LIGO Scientific CollaborationThe Virgo CollaborationThe KAGRA
  Collaboration, et al. 2021, arXiv:2111.03606
The LIGO Scientific CollaborationThe Virgo CollaborationThe KAGRA
  Collaboration, et al. 2023, ApJS, 267, 29
Tichy, W., & Marronetti, P. 2008, PhRvD, 78, 081501
Tong, H., Galaudage, S., & Thrane, E. 2022, PhRvD, 106, 103019
Tutukov, A. V., & Yungelson, L. R. 1993, MNRAS, 260, 675
van den Heuvel, E. P. J. 1976, in IAU Symp. 73, Structure and Evolution of
  Close Binary Systems, ed. P. Eggleton, S. Mitton, & J. Whelan (Dordrecht:
  D. Reidel), 35
van den Heuvel, E. P. J., Portegies Zwart, S. F., & de Mink, S. E. 2017,
   MNRAS, 471, 4256
Woosley, S. E. 2017, ApJ, 836, 244
Woosley, S. E., Blinnikov, S., & Heger, A. 2007, Natur, 450, 390
```